AVE Trends in Intelligent Informatics Reports

An Intelligent Noise Suppression Algorithm for Multi-Purpose Imaging Systems

R. Remya[1,*], O. Jeba Singh[2], J. Angelin Jeba[3], S. Rubin Bose[4], R. Regin[5], M. Mohamed Sameer Ali[6]

[1]Department of Electronics and Communication Engineering, Sri Krishna College of Engineering and Technology, Coimbatore, Tamil Nadu, India.
[2]Centre for Academic Research, Alliance University, Bengaluru, Karnataka, India.
[3]Department of Electronics and Communication Engineering, S.A. Engineering College, Chennai, Tamil Nadu, India.
[4,5]School of Computer Science Engineering, SRM Institute of Science and Technology, Ramapuram, Chennai, Tamil Nadu, India.
[6]Department of Research and Development, Dhaanish Ahmed College of Engineering, Chennai, Tamil Nadu, India.
remiamernath@gmail.com[1], jeba.singh@alliance.edu.in[2], angelinjeba@saec.edu.in[3], rubinbos@srmist.edu.in[4], reginr@srmist.edu.in[5], sameerali7650@gmail.com[6]

*Corresponding author

Abstract: Image denoising is very important for getting better image quality so that you can analyze and understand it correctly. Various evaluation metrics are used to assess how well filtering techniques work and provide reliable quality assessments. This study introduces an innovative denoising technique for versatile images across various application domains. The filtered output generated by the proposed technique serves as a crucial preprocessing step for subsequent processes, including segmentation, feature extraction, and classification, where noise-free data markedly improves performance. Researchers use well-known quantitative measures, such as Peak Signal-to-Noise Ratio (PSNR), Normalized Absolute Error (NAE), and Structural Similarity Index Measure (SSIM), to assess the quality of denoised images. Researchers perform experimental analysis on a wide range of image types, including remote sensing, medical, and standard benchmark images such as Barbara, Cameraman, vegetable, and scenic. The results show that the new enhanced discrete wavelet transform (DWT)–based method outperforms other denoising methods for filtering. The improved DWT method, in particular, provides about 0.2% better filtering efficiency across all datasets tested. In general, the results show that the proposed denoising framework consistently improves image quality and effectively supports advanced image processing tasks in medical imaging, remote sensing, and general computer vision applications.

Keywords: Image Filtering; Image Denoising; Rician Noise; Similarity Index Measure (SSIM); Normalized Absolute Error (NAE); Computer Vision; Discrete Wavelet Transform (DWT).

Cite as: R. Remya, O. J. Singh, J. A. Jeba, S. R. Bose, R. Regin, and M.M.S. Ali, "An Intelligent Noise Suppression Algorithm for Multi-Purpose Imaging Systems," *AVE Trends in Intelligent Informatics Reports*, vol. 1, no. 1, pp. 37–51, 2026.

Journal Homepage: https://www.avepubs.com/user/journals/details/ATIIR

Received on: 18/04/2025, **Revised on:** 05/06/2025, **Accepted on:** 06/08/2025, **Published on:** 01/03/2026

DOI: https://doi.org/10.64091/ATIIR.2026.000279

1. Introduction

Pre-processing an image is essential for improving its quality and enabling analysis. In image processing, pre-processing is a major step that improves image quality by removing noise from a raw image. Normally, medical images captured via Magnetic Resonance Imaging (MRI), Computer Tomography (CT), Ultrasound (US), and X-ray are contaminated with noise [1]. In particular, MRI images are affected by Rician noise, making it difficult for clinicians to identify the structures of human organs and tissues. Denoising can be performed in the spatial or frequency domain. In the spatial domain, the operations are performed directly on image pixels. But in the transform domain, images are converted to the frequency domain via transformations such as wavelets or the Fourier transform. The different types of denoising include spatial and temporal domains [2]. Under the transform or temporal method, the frequency and wavelet methods can be adopted. The above approaches are applied to various types of noise. The work primarily focuses on removing Rician noise, which is discussed in subsequent sections. There are multiple denoising methods; one such method is anisotropic filtering, which falls under the Diffusion filtering category [3]. This method helps suppress noise without blurring essential edges. It adjusts the diffusion based on local gradients, which makes it better suited to Gaussian noise. But, the performance is limited for impulse, speckle and mixed noises. Another method is the Nonlocal Mean (NLM) filter approach [4]. It compares patches across the entire image and preserves superior detail and high quality. This method is excellent for Gaussian noise; however, the nonlocal mean variant approach has several drawbacks, including a high computational burden, sensitivity to noise variations, and the need for a hybrid approach for large-scale and real-time applications. In which the texture information is protected [5]. Moreover, a weighted nuclear-norm-based normalization method is proposed to address several practical denoising problems.

2. Review of Literature

According to Onyedinma and Onyenwe [6], a comparative analysis of various spatial filtering techniques for image denoising is presented. Different filtering techniques, such as the Average Mean Filter, Median Filter, Gaussian Filter and Bilateral Filter, are analyzed. The evaluation of these filters is made through MSE, PSNR, SSIM, RMSE and UQI metrics. Moreover, Priya et al. [7] presented a methodology to eliminate four types of image noise: Speckle, Poisson, Salt-and-Pepper, and Amplifier. Different noise reduction models, including the Wiener filter, Inverse filter and Luyfin Richardson method, improve the image quality. The performances are evaluated through MSE and PSNR metrics. Furthermore, Ullah et al. [8] introduced a hybrid denoising algorithm that combines the Modified Decision-Based Median Filter (MDBMF) and the Adaptive Median Filter (AMF). The AMF will adjust the window size to identify the noisy pixels. A quantitative evaluation is performed using standard datasets, such as chest and Liver images with varying noise levels. In addition, Xiao et al. [9] developed and implemented a computational model of Weighted Mean Filtering parallel algorithm for open CL. The parallel algorithm is implemented at two levels: work items and groups. This technique provides better computational performance across different GPUs. According to Capobianco et al. [10], a new approach to retrieve the image after convolution is presented.

The deconvolution is performed in three steps: first, identify the filter; then minimize the mean absolute error; and finally, identify the filter again. Another study introduces a filtering technique in Mohanty and Tripathy [11] to remove image noise. Linear, non-linear and adaptive filters are implemented to reduce noise such as salt-and-pepper, Gaussian, sparkle and Poisson noise. MSE and PSNR values are used to evaluate the system's performance. According to the literature survey, the frequency-domain method is more suitable for Rician noise removal. Similarly, the wavelet-based approach is well-suited for preserving image edges and fine details. In the case of medical images, the fine details should be considered. The filtering quality is justified based on the performance metrics. To measure performance metrics, the filtered image is compared with the ground truth image [12]. In this work, a new performance metric is proposed, along with existing metrics such as PSNR, NAE and SSIM. Rician noise in MRI images corrupts the information; hence, this work primarily focuses on removing it. Finally, a comparative analysis is made between the Enhanced Discrete Wavelet Transform (EDWT) and other existing methods with a common publicly available data set. The objective and contribution of this work:

- To perform filtering to remove Rician Noise.
- To evaluate performance using traditional metrics as well as novel performance metrics.
- To conduct a comparative analysis with different denoising methods.

3. Proposed Methodology

The proposed flow diagram of this method is depicted in Figure 1. As per the methodology, normal MR images are used as input for processing. In a few cases, the MR images obtained may be corrupted by Rician noise. For other images, researchers may add Rician noise for analytical purposes. The noisy images are then filtered [13]. The enhanced DWT removes Rician noise [14]. Finally, the performances are calculated through the metrics for the filtered output [22].

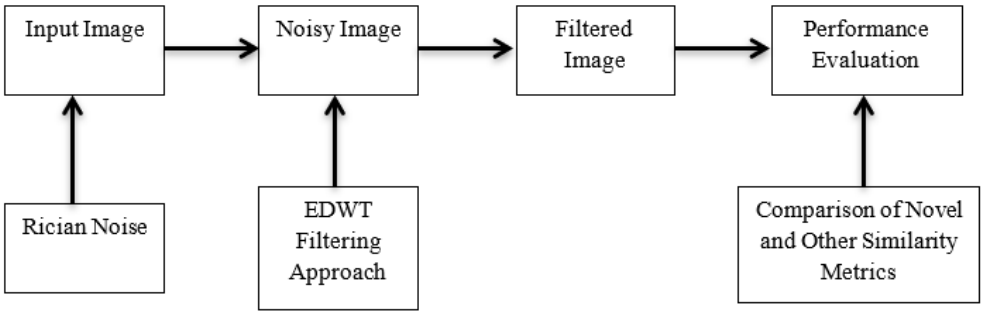

Figure 1: Proposed flow of work

If noise is present in the input image, the quality of the output is affected when it is enhanced, segmented or classified. Moreover, it reduces the filtering process's performance. In our case study, publicly available datasets, such as the BRATS dataset, were used. Also, some common images like Cameraman, Barbara, Satellite, Vegetables and Scenic images are also processed. Initially, when Rician noises are included with the input images. Therefore, the Rician noise distribution is given by equation (1):

$$R(d) = \frac{p}{q^2} exp\left(-\frac{p^2+P^2}{2q^2}\right).J\left(\frac{pP}{q^2}\right) \quad (1)$$

Where R(d) is the Rician noise distribution, 'p' stands for the magnitude of the image, 'q' refers to the standard distribution, 'P' is the pure input image, and 'J' stands for the Bessel function of order zero. The same distribution can be used whenever noise is evaluated. Generally, for image analysis and for calculating the Signal to Noise Ratio (SNR), the image foreground is chosen. Otherwise, the image background is preferred for calculating the noise variance, especially when the SNR is at its minimum [15]. At this stage, the Rician distribution will function like a Rayleigh distribution in the case of background content, and the Rayleigh distribution is given by:

$$R(R) = \frac{x}{y^2} exp\left(-\frac{x^2}{2y^2}\right) \quad (2)$$

Where x is the mean and y is the variance of the background information. The background mean and variance are expressed in equations (3) and (4), respectively:

$$x_b = y.\sqrt{\frac{\pi}{2}} \quad (3)$$

$$y_b = y^2 \frac{4-\pi}{2} \quad (4)$$

Equations (3) and (4) are not valid if any artifacts are present in the image. It is required to minimize image noise to avoid performance degradation during image analysis. Therefore, filtering methods are applied to eliminate the noise from the image. In the preprocessing stage, image filtering is a key step of image analysis. In which selecting the suitable filter for the particular noise is more challenging [16]. In the proposed scheme, an algorithm is highlighted that efficiently removes the Rician noise. Among the various filtering methods experimented with for Rician noise removal, the Discrete Wavelet Transform (DWT) is found to be suitable. Here, the DWT is enhanced by a modified technique named the Enhanced Discrete Wavelet Transform (EDWT).

3.1. Enhanced Discrete Wavelet Transform (EDWT)

DWT is mostly used due to its advantages, such as the preservation of image information during filtering [17]. Also, in DWT, the image is decomposed into subbands, including Very Low (VL), Low (L), High (H), and Very High (VH). Among these, the VL sub-band provides the accurate information content required for future analysis. As per our procedure, DWT is applied to the image first. The approximation coefficient of DWT is given by:

$$W_{\emptyset}(i,T_1,T_2) = \frac{1}{\sqrt{Q_1 Q_2}} \sum_{Q_1=0}^{Q_1-1} \sum_{Q_1=0}^{Q_2-1} t(Q_1,Q_2) \emptyset_{i,T_1,T_2} \quad (5)$$

Similarly, horizontal, vertical and diagonal coefficients are expressed as:

$$W_{\psi}{}^{j}(i,T_1,T_2) = \frac{I}{\sqrt{Q_1Q_2}}\sum_{Q_1=0}^{Q_1-1}\sum_{Q=0}^{Q_2-1} t(Q_1,Q_2)\psi_{i,T_1,T_2}^{j} \quad (6)$$

Here, variable 'j' denotes the coefficients that belong to either horizontal 'H', vertical 'V', or diagonal 'D'; j = {H, V, D}. Likewise, the size of the images is represented as Q_1 and Q_2. Similarly, T_1 and T_2 represent the translation of the wavelet coefficients. Let the scaling function be 'Ø', the wavelet function be Ψ, and the parameter that affects the scaling function is denoted as 'I'. In thresholding, two processes occur depending on the threshold value: soft and hard thresholding. Then, by comparing hard and soft thresholding, the latter is preferred to reduce irregularity issues [18]. As a result, the value for soft threshold is expressed as:

$$g = \frac{1}{qw}.\frac{\sum_{z=1}^{q}\sum_{z'=1}^{w} s_{zz\prime}^{3}}{\sum_{z=1}^{q}\sum_{z'=1}^{w} s_{zz\prime}} \quad (7)$$

Here, q and w represent the size of the image, $s_{zz\prime}$ is the pixel value at location (z, z'). Once the soft threshold is obtained, check whether it exceeds the threshold; if so, it will be considered for the analysis. Accordingly, a soft thresholding function based on the proposed threshold is calculated using equation (8):

$$(st) = \frac{1}{1+d\prime^2}.signum\big(c(|c| - g)\big) \quad (8)$$

In the above thresholding function, a new signum function is utilized. The value of the signum function is chosen as '1' if the input is greater than zero. Also, the value of the signum function is chosen as '0' if the input is less than zero [19]. In case the input is less than zero, then d^1 is the average of the lowest and highest value of the input image selected for filtering and is represented as in equation (9):

$$d' = \frac{\max(P)+\min(P)}{2} \quad (9)$$

Finally, by calculating the threshold, the inverse DWT is obtained. Thus, researchers can obtain the denoised image. In the output, information such as edge details is preserved in the image [20]. The Inverse Discrete Wavelet Transform (IDWT) is given as in equation (10):

$$t(T_1,T_2) = \frac{1}{\sqrt{Q_1Q_2}}\sum_{j=\{H,V,D\}}\sum_{i=0}^{\infty}\sum_{T_1}\sum_{T_2} W_{\emptyset}(i,T_1,T_2)\,\emptyset_{i,T_1,T_2} + \frac{1}{\sqrt{Q_1Q_2}}\sum_{j=\{H,V,D\}}\sum_{i=0}^{\infty}\sum_{T_1}\sum_{T_2} W_{\psi}{}^{j}(i,T_1,T_2)\,\psi_{i,T_1,T_2}^{j} \quad (10)$$

Finally, the denoised image is measured to justify the denoising process. Moreover, performance analysis is made based on traditional metrics and proposed novel similarity metrics.

3.2. Performance/ Similarity Metrics

Along with common performance metrics such as PSNR, NAE and SSIM, a novel similarity metric is also proposed to assess performance. This metric is primarily based on the logarithm (Lg). The logarithmic function is the ratio between the maximum pixel value obtained from the filtered image and the logarithmic function Lgn calculated between the input and the filtered image [21]. The proposed evaluation metric Lg is represented by (11) as:

$$Lg = 20 \times log10\left(\frac{L_{max}}{Lgn}\right) \quad (11)$$

$$Lgn(i,j) = \sum_{j=1}^{L}\sum_{i=1}^{m}\frac{\log\big(I(j,i)\big)-\log\big(N(j,i)\big)}{\sqrt{\log\big(I(j,i)\big)\times\log\big(N(j,i)\big)}} \quad (12)$$

Where L_{max} is the maximum pixel value, lg logarithmic similarity metric, Lgn is the ratio of the average difference between the input and filtered image pixels to the square root of the pixel product of the input and filtered image. $I(j,i)$ is the input image, $N(j,i)$ filtered image as in equation (12). The performance improvement is predicted based on the logarithm of the value. A high logarithmic function value indicates a good similarity index; a low one, poor performance. Steps to compute the proposed logarithmic similarity metric:

- **Step 1:** The similarity metric is calculated pixel-wise throughout the image.

- **Step 2:** Add all the results pixelwise to get the similarity metric for the entire image.
- **Step 3:** If the metric value falls within the range of 60-75, the image is considered high-quality; otherwise, it is low-quality.

After obtaining the similarity metric, an inference is made based on the accuracy, similarity measure, computation time and generalization. The conventional similarity metric, PSNR, is defined in terms of the MSE. It is inversely proportional to MSE, and the error is calculated as the average squared deviation between the input and the filtered image. Higher PSNR indicates less error, and lower PSNR indicates more error. The PSNR is calculated using equation (13):

$$PSNR = 10log_{10}\frac{255^2}{MSE,} \tag{13}$$

$$PSNR = 10log_{10}\frac{255^2}{MSE,} \tag{14}$$

Structural Similarity Index is defined based on the distortion value of correlation, contrast and luminance represented in equation (15):

$$SM = LD(I,N)CR(I,N)CD(I,N) \tag{15}$$

$$\begin{cases} LD(I,N) = \frac{2M_IM_N+K_1}{M_I^2+M_N^2+K_1} \\ CD(I,N) = \frac{2V_IV_N+K_2}{V_I^2+V_N^2+K_2} \\ CR(I,N) = \frac{V+K_3}{V_I+V_N+K_3} \end{cases} \tag{16}$$

The distortion types, like luminance $LD(I,N)$, correlation $CR(I,N)$ and contrast $CD(I,N)$ can be obtained from equation (16). Here, mean values are denoted as M_I and M_N, and the standard deviation is represented as V_I and V_NFor example, V_{IN} is the covariance value of the images I and N. Also, K_1, K_2 and K_3 These are the constants. The value of Structural Measure (SM) must be within the range of 0 and 1. Finally, the Normalized Absolute Error (NAE) is defined as the difference between the testing image and the filtered response. The value of NAE lies between 0 and ∞. If the obtained measure is close to zero, it indicates that the image is of higher quality. If the obtained measure is nearer to infinity, it indicates that the filtered response is of poor quality. The NAE equation is given as in equation (17):

$$N = \frac{\sum_{j=1}^{M}\sum_{i=1}^{m}|I(j,i)-N(j,i)|}{\sum_{j=1}^{M}\sum_{i=1}^{m}I(j,i)} \tag{17}$$

4. Results and Discussion

The simulations were carried out on MATLAB. In this section, the proposed enhanced DWT method is implemented, and the results are compared with those of other filtering techniques, such as the median filter and the Berkeley Wavelet Transform (BWT). Initially, the input images are added to Rician noise at noise levels of 10, 20, 30, 40 and 50 dB. Then, denoising is performed using the Enhanced Wavelet Transform. In addition, the Daubechies Wavelet is applied to smooth the image based on the wavelet order (N). During this process, selecting the order of the filter plays an important role. In our case, a two-level decomposition is used for image filtering with N=2.

4.1. Case 1: Cameraman Image

In case 1, the Cameraman image is taken as the input. After denoising, the obtained outputs are depicted in Figure 2. The noise-added image is shown in Figure 2(b), and the filtered output using the enhanced DWT is shown in Figure 2(c). Likewise, the filtered outputs using existing transforms, such as the Berkeley Wavelet Transform (BWT), Standard DWT filter, Lee filter, Frost filter and Weiner filter, are shown in Figures 2(d-h), respectively. When analyzing the outputs of the proposed method compared with other filtering methods, the enhanced wavelet approach effectively preserves image content and reduces noise. The performance metrics are calculated for the proposed method and other filtering approaches, such as the standard DWT, BWT, Lee, Frost and Weiner. When evaluating metrics such as PSNR, NAE, SSIM, and the proposed similarity metric, the NAE value is about 0.0062 for the proposed filter with 50% Rician noise; it is 0.0058 with 40% added to the input, and 0.0053withr 30% added. Furthermore, in the 20% and 10% noise conditions, the enhanced DWT method achieves greater accuracy than other algorithms.

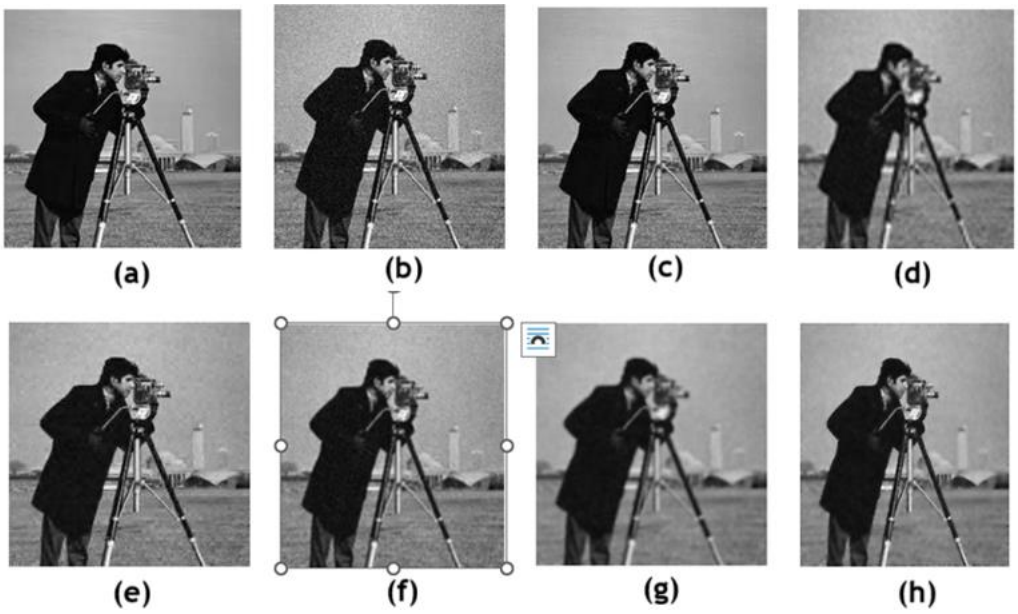

Figure 2: (a) Input image, (b) Noisy image, (c) Enhanced DWT, (d) BWT, (e) DWT, (f) Lee, (g) Frost, (h) Weiner

This result shows that there is no disruption in the image content. The value of NAE should be as low as possible, indicating a high-quality filtered response. The complete responses by all methods are tabulated in Table 1. The estimated PSNR metric is also included in Table 1. The estimated accuracy, as measured by the PSNR metric, for the enhanced DWT technique is higher than that of the standard DWT, BWT, Lee, Frost and Weiner algorithms by 50.32%, 20.77%, 47.04%, 39.77% and 45.17%, respectively. Furthermore, the accuracy is better with other approaches for 40%, 30%, 20%, and 10% noise levels. In addition, the performance estimated using the SSIM metric is good for all noise levels from 50% to 10%.

Table 1: Existing and proposed metric values on cameraman images

Parameter	Noise Level	DWT	BWT	Lee	Frost	Weiner	Proposed Method
NAE	10%	0.067	0.022	0.050	0.067	0.0448	0.0045
	20%	0.076	0.022	0.060	0.077	0.0546	0.0049
	30%	0.086	0.022	0.071	0.087	0.0645	0.0054
	40%	0.096	0.022	0.083	0.098	0.0753	0.0059
	50%	0.107	0.022	0.094	0.109	0.0876	0.0063
PSNR	10%	25.315	38.070	27.985	34.712	30.550	48.670
	20%	25.218	38.172	27.486	33.204	29.612	48.669
	30%	25.212	38.101	26.891	31.639	28.542	48.561
	40%	24.493	38.126	25.905	29.981	27.544	48.254
	50%	23.927	38.162	25.510	29.008	26.413	48.169
SSIM	10%	0.772	0.942	0.859	0.757	0.814	0.999
	20%	0.677	0.942	0.760	0.655	0.715	0.996
	30%	0.582	0.943	0.666	0.558	0.624	0.997
	40%	0.509	0.943	0.590	0.482	0.546	0.999
	50%	0.450	0.943	0.531	0.421	0.488	0.998
Proposed Metric	10%	40.660	48.317	43.037	41.270	43.603	60.498
	20%	39.970	48.437	41.513	40.341	42.101	60.403
	30%	39.574	48.339	40.580	39.335	41.065	60.400
	40%	38.834	48.456	39.610	38.854	40.389	60.292
	50%	38.358	48.436	39.445	38.478	39.715	60.518

Though the image is of low quality, the proposed DWT method achieves an SSIM value of 60.51. The result is superior to those of other methods, such as standard DWT, BWT, Lee, Frost and Weiner, by 36.62%, 19.97%, 34.82%, 36.42% and 34.74%, respectively. Since the SSIM value is close to 1, the accuracy is higher.

4.2. Case 2: Barbara Image

Under case study 2, the performance of the proposed filter is tested with a Barbara image. The original input image, noise-added image, and filtered images are displayed in Figure 3. Here, the original Barbara image is provided in Figure 3(a), the noise-added image in Figure 3(b), the proposed filter output in Figure 3(c), and the results of other methodologies, including standard DWT, BWT, Lee, Frost, and the Wiener filters, are presented in Figure 3(d-h).

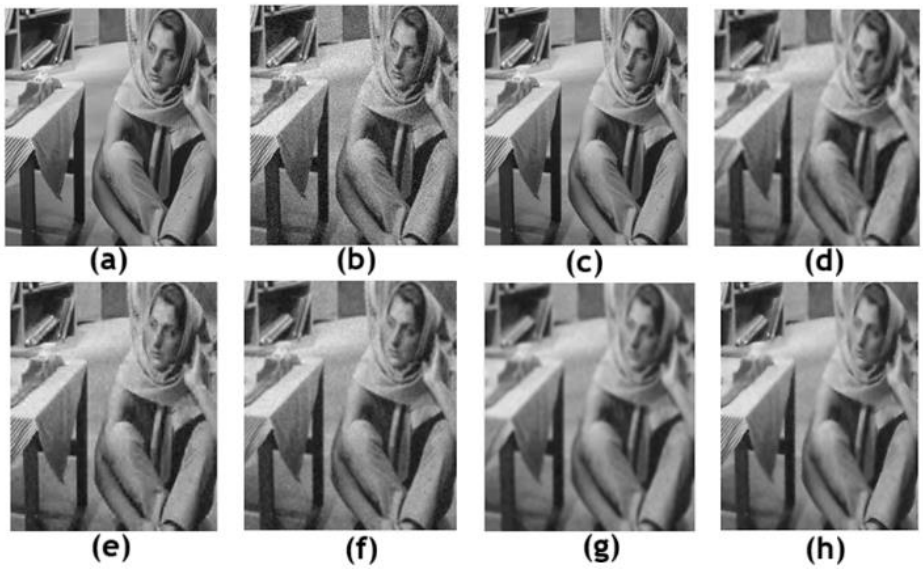

Figure 3: (a) Input image, (b) Noisy image, (c) Enhanced DWT, (d) BWT, (e) DWT, (f) Lee, (g) Frost, (h) Weiner

The obtained evaluation metrics, like NAE, PSNR and SSIM, are tabulated in Table 2. The average NAE for the proposed enhanced DWT method is 0.0053, which is much smaller than those of other methods, indicating an enhanced filtering approach. Likewise, the average PSNR is about 49.4372, which is much better than the other methods.

Table 2: Existing and proposed metric values for Barbara images

Parameter	Noise Level	DWT	BWT	Lee	Frost	Weiner	Proposed Method
NAE	10%	0.068	0.034	0.052	0.0745	0.056	0.005
	20%	0.076	0.043	0.061	0.082	0.063	0.005
	30%	0.085	0.054	0.072	0.102	0.073	0.005
	40%	0.097	0.065	0.085	0.102	0.084	0.006
	50%	0.109	0.075	0.098	0.113	0.095	0.006
PSNR	10%	26.475	34.300	28.920	26.011	29.116	50.080
	20%	26.101	32.163	27.970	25.878	28.555	49.860
	30%	25.794	30.390	26.810	25.172	27.435	49.408
	40%	25.097	28.776	26.466	24.302	26.506	49.254
	50%	24.226	27.744	25.361	23.966	25.679	48.585
SSIM	10%	0.766	0.928	0.844	0.738	0.805	0.999
	20%	0.712	0.882	0.786	0.681	0.749	0.999
	30%	0.651	0.836	0.720	0.614	0.686	0.999
	40%	0.587	0.799	0.657	0.553	0.624	0.999
	50%	0.532	0.768	0.601	0.499	0.567	0.999
Proposed metric	10%	44.056	49.780	46.676	43.505	45.604	67.003
	20%	43.129	47.528	44.848	42.847	44.613	66.405
	30%	42.330	45.693	43.137	41.735	43.214	65.579
	40%	41.306	43.995	42.430	40.516	42.069	64.983
	50%	40.218	42.905	41.167	39.955	41.215	63.802

The next value for BWT is only 30.6745. Moreover, the SSIM value is about 0.9991, indicating a higher result, and the average value is 65.5544. Therefore, for any image at any noise level up to 50%, the proposed DWT method provides better results in reducing the Recian noise.

4.3. Case 3: Remote Sensing Image

In case 3, the Remote sensing image is taken as the input. After denoising, the obtained outputs are depicted in Figure 4. The noise-added image is shown in Figure 4(b), and the filtered output using the enhanced DWT is shown in Figure 4(c). Likewise, the filtered outputs using existing transforms, such as the Berkeley Wavelet Transform (BWT), Standard DWT filter, Lee filter, Frost filter and Weiner filter, are shown in Figure 4(d-h), respectively.

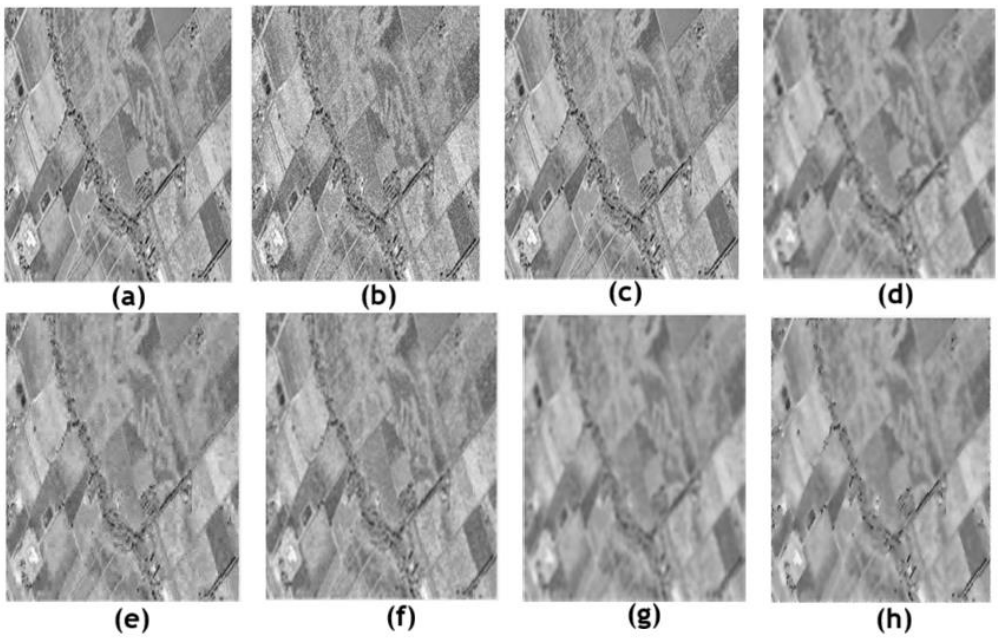

Figure 4: (a) Input image, (b) Noisy image, (c) Enhanced DWT, (d) BWT, (e) DWT, (f) Lee, (g) Frost, (h) Weiner

The performance of the enhanced algorithms has been evaluated using various metrics, as shown in Table 3. It shows that across all performance metrics, enhanced DWT yields better results than the standard DWT, BWT, Lee, Frost, and Weiner algorithms.

Table 3: Existing and proposed metric values for remote sensing images

Parameter	Noise Level	DWT	BWT	Lee	Frost	Weiner	Proposed Method
NAE	10%	0.066	0.044	0.050	0.071	0.058	0.004
	20%	0.070	0.048	0.056	0.076	0.062	0.004
	30%	0.076	0.054	0.063	0.082	0.068	0.005
	40%	0.084	0.060	0.071	0.089	0.075	0.005
	50%	0.09	0.067	0.081	0.097	0.083	0.005
PSNR	10%	25.033	29.640	27.320	24.406	26.946	49.332
	20%	24.794	29.119	26.898	24.245	26.592	49.221
	30%	24.538	28.479	26.393	23.794	26.195	49.055
	40%	24.086	27.783	25.751	23.684	25.480	48.564
	50%	23.599	27.048	24.631	23.071	24.680	48.348
SSIM	10%	0.628	0.816	0.781	0.550	0.657	0.999
	20%	0.593	0.793	0.738	0.513	0.622	0.999
	30%	0.546	0.765	0.684	0.465	0.574	0.999
	40%	0.495	0.737	0.629	0.421	0.524	0.999
	50%	0.448	0.710	0.572	0.376	0.481	0.999
	10%	41.152	44.753	43.354	40.391	42.510	64.950

Proposed metric	20%	40.741	44.186	42.675	40.086	42.066	64.730
	30%	40.292	43.534	41.959	39.469	41.588	64.465
	40%	39.646	42.840	41.152	39.218	40.810	63.795
	50%	39.049	42.078	39.936	38.483	39.976	63.480

4.4. Case 4: Vegetable Image

In case 4, the Vegetable image is taken as the input. After denoising, the obtained outputs are depicted in Figure 5. The noise-added image is shown in Figure 5(b), and the filtered output using the enhanced DWT is shown in Figure 5(c). Likewise, the filtered outputs using existing transforms such as the Berkeley Wavelet Transform (BWT), Standard DWT filter, Lee filter, Frost filter and Weiner filter are shown in Figure 5(d-h), respectively.

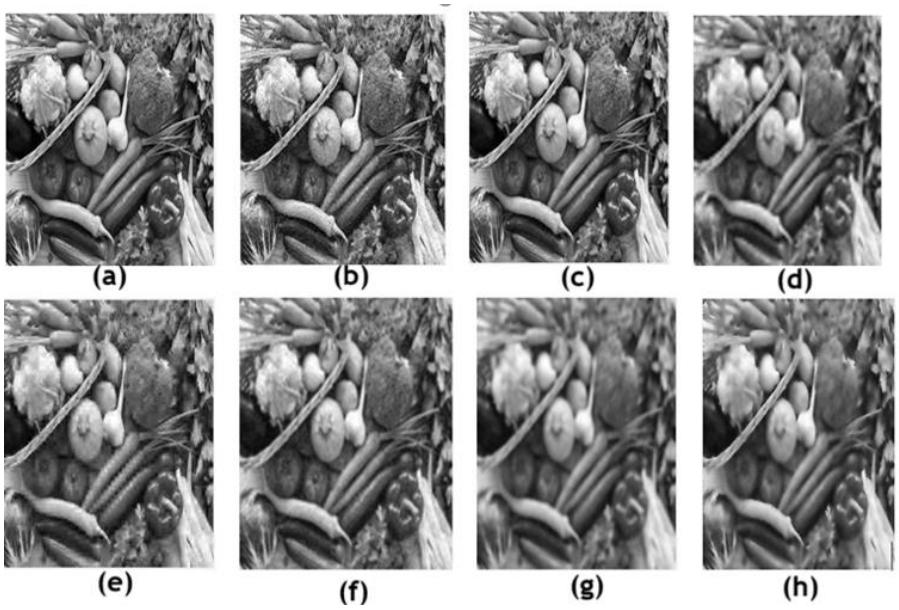

Figure 5: (a) Input image, (b) Noisy image, (c) Enhanced DWT, (d) BWT, (e) DWT, (f) Lee, (g) Frost, (h) Weiner

Different algorithms are tested at levels ranging from 10% to 50% to select the appropriate filter for a given noise level. However, various algorithms, such as the enhanced DWT, standard DWT, BWT, Lee, Frost, and Weiner, are utilized to assess the consistency in the noise content. The response to various filtering approaches is depicted in Table 4.

Table 4: Existing and proposed metric values for vegetable images

Parameter	Noise Level	DWT	BWT	Lee	Frost	Weiner	Proposed Method
NAE	10%	0.119	0.071	0.087	0.127	0.099	0.008
	20%	0.123	0.077	0.093	0.132	0.104	0.008
	30%	0.130	0.084	0.102	0.138	0.110	0.009
	40%	0.138	0.092	0.111	0.145	0.118	0.009
	50%	0.148	0.100	0.122	0.154	0.127	0.009
PSNR	10%	22.528	28.250	25.243	22.154	24.875	45.951
	20%	22.706	27.894	25.043	22.343	24.720	45.935
	30%	22.537	27.390	24.835	22.140	24.550	46.066
	40%	22.219	26.579	24.326	22.089	24.274	46.127
	50%	22.164	26.283	23.849	21.896	23.867	46.248
SSIM	10%	0.710	0.885	0.840	0.373	0.753	0.999
	20%	0.389	0.865	0.815	0.651	0.730	0.999
	30%	0.661	0.842	0.780	0.620	0.701	0.999
	40%	0.626	0.818	0.743	0.588	0.668	0.999
	50%	0.589	0.799	0.705	0.554	0.632	0.999
	10%	39.298	42.654	41.959	38.958	40.467	60.467

Proposed metric	20%	39.333	42.459	41.435	38.963	40.208	60.531
	30%	39.017	42.022	40.900	38.577	39.937	60.628
	40%	38.483	41.346	40.173	38.359	39.579	60.767
	50%	38.293	41.158	39.587	38.058	39.186	60.793

4.5. Case 5: Nature Image

In case 5, the Nature image is taken as the input. After denoising, the obtained outputs are depicted in Figure 6. The noise-added image is shown in Figure 6(b), and the filtered output using the enhanced DWT is shown in Figure 6(c). Likewise, the filtered outputs using existing transforms such as the BWT, Standard DWT filter, Lee filter, Frost filter and Weiner filter are shown in Figure 6(d-h), respectively.

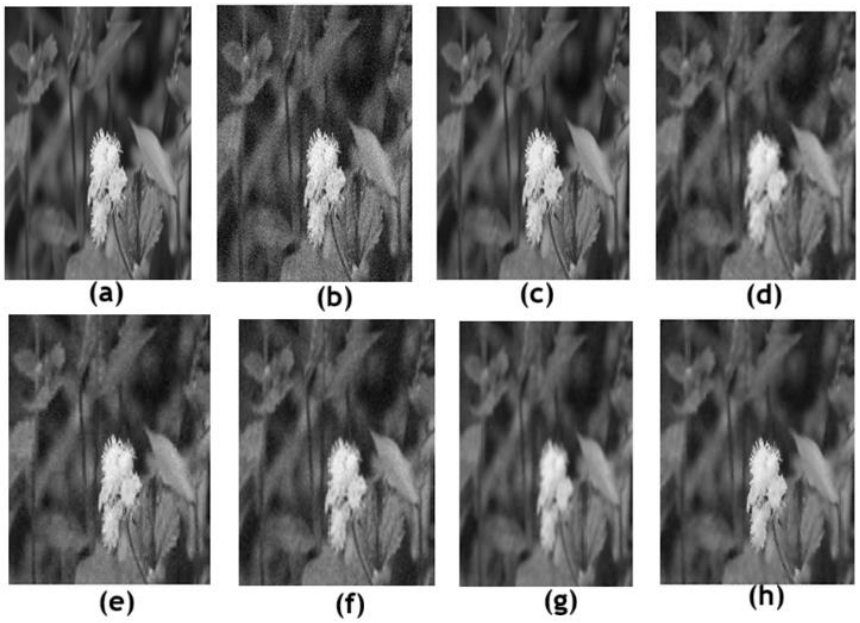

Figure 6: Natural image, (a) Input image, (b) Noisy image, (c) Enhanced DWT, (d) BWT, (e) DWT, (f) Lee, (g) Frost, (h) Weiner

The similarity metric analyzes the performance. In this similarity estimation, quantitative evaluations from various approaches are depicted in a line chart. It shows that the enhanced DWT performs well across all performance measures (Table 5).

Table 5: Existing and proposed metric values for natural images

Parameter	Noise Level	DWT	BWT	Lee	Frost	Weiner	Proposed Method
NAE	10%	0.047	0.028	0.037	0.056	0.041	0.003
	20%	0.065	0.044	0.056	0.071	0.057	0.004
	30%	0.084	0.060	0.077	0.089	0.075	0.005
	40%	0.104	0.076	0.097	0.109	0.095	0.006
	50%	0.123	0.091	0.118	0.128	0.113	0.007
PSNR	10%	31.156	38.180	33.652	30.193	34.538	54.211
	20%	30.059	34.850	31.724	29.120	32.284	53.653
	30%	28.440	32.601	29.693	28.099	29.997	52.816
	40%	27.077	30.287	27.871	26.920	28.308	52.081
	50%	26.394	28.86	26.496	25.697	26.890	50.978
SSIM	10%	0.892	0.950	0.930	0.866	0.904	0.100
	20%	0.797	0.894	0.837	0.770	0.810	0.999
	30%	0.693	0.836	0.729	0.662	0.703	0.999
	40%	0.596	0.784	0.636	0.562	0.609	0.999
	50%	0.517	0.747	0.561	0.484	0.533	0.999

Proposed metric	10%	51.153	54.269	53.107	49.847	51.520	73.925
	20%	47.998	50.647	49.067	47.139	48.412	71.898
	30%	45.418	48.236	46.166	45.190	45.859	70.015
	40%	43.564	45.843	43.994	43.467	44.056	68.469
	50%	42.612	44.351	42.438	41.976	42.567	66.752

4.6. Case study 6: Corona-Infected Lung Image

The experiment in case study 6 is conducted on a corona-infected image collected from the Kaggle dataset, and the outcomes of various filtering approaches are shown in Figure 7. The noise-added image is shown in Figure 7(b), and the filtered output using the enhanced DWT is shown in Figure 7(c). Likewise, the filtered outputs using existing transforms, such as the Berkeley Wavelet Transform (BWT), Standard DWT filter, Lee filter, Frost filter and Weiner filter, are shown in Figure 7(d-h), respectively.

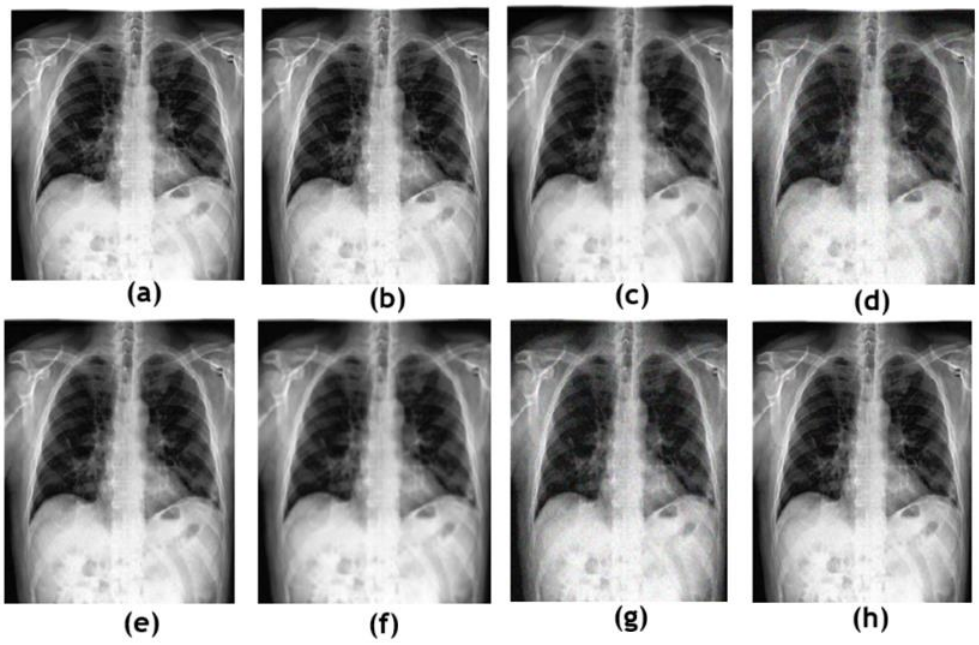

Figure 7: (a) Input image, (b) Noisy image, (c) Enhanced DWT, (d) BWT, (e) DWT, (f) Lee, (g) Frost, (h) Weiner

The performance of the various algorithms has been analyzed using similarity metrics, and the results are depicted in Table 6.

Table 6: Existing and proposed metric values for the corona-infected image

Parameter	Noise Level	DWT	BWT	Lee	Frost	Weiner	Proposed Method
NAE	10%	0.128	0.057	0.099	0.139	0.094	0.010
	20%	0.179	0.096	0.148	0.168	0.129	0.009
	30%	0.194	0.127	0.173	0.206	0.159	0.012
	40%	0.219	0.149	0.208	0.218	0.193	0.016
	50%	0.221	0.178	0.243	0.249	0.206	0.017
PSNR	10%	32.810	34.479	28.468	30.488	35.787	39.348
	20%	31.643	29.479	27.566	29.766	34.799	38.435
	30%	30.668	26.669	26.459	27.699	34.136	37.588
	40%	29.403	23.579	24.787	26.098	33.676	34.588
	50%	28.143	22.577	22.675	24.787	32.113	33.981
SSIM	10%	0.895	0.966	0.906	0.868	0.905	0.100
	20%	0.755	0.915	0.817	0.795	0.816	0.100
	30%	0.599	0.851	0.712	0.685	0.705	0.999
	40%	0.568	0.784	0.612	0.594	0.618	0.999
	50%	0.510	0.735	0.512	0.497	0.538	0.999

Proposed metric	10%	22.578	25.679	23.898	23.895	23.452	44.689
	20%	21.577	44.447	42.435	42.510	42.490	44.234
	30%	21.231	43.726	41.790	41.626	41.795	44.079
	40%	20.676	43.022	41.084	41.000	41.134	43.782
	50%	20.234	42.372	40.870	40.211	40.438	43.126

4.7. Case study 7: Brain Tumor Image

In case study 7, the brain tumor image is used as the input. These images were collected from the BRATS dataset. After denoising, the obtained outputs are depicted in Figure 8. The noise-added image is shown in Figure 8(b), and the filtered output using the enhanced DWT is shown in Figure 8(c). Likewise, the filtered outputs using existing transforms such as the Berkeley Wavelet Transform (BWT), Standard DWT filter, Lee filter, Frost filter and Weiner filter are shown in Figure 8(d-h), respectively.

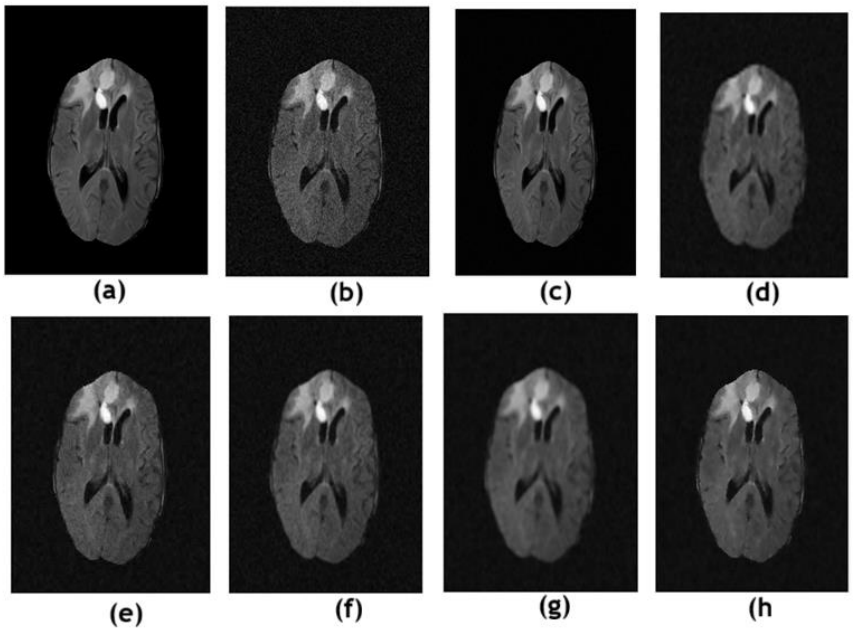

Figure 8: (a) Input image, (b) Noisy image, (c) Enhanced DWT, (d) BWT, (e) DWT, (f) Lee, (g) Frost, (h) Weiner

The performance analysis of the various algorithms has been conducted using the similarity metrics; the results are depicted in Table 7. The value of NAE should be as low as possible. In Table 7, the enhanced DWT approach yields a lower value than the other approaches. Similarly, the PSNR and SSIM values are higher for the proposed algorithm.

Table 7: Existing and proposed metric values for BRATS images

Parameter	Noise Level	DWT	BWT	Lee	Frost	Weiner	Proposed Method
NAE	10%	0.119	0.049	0.098	0.121	0.081	0.008
	20%	0.151	0.084	0.134	0.152	0.117	0.009
	30%	0.181	0.113	0.167	0.182	0.149	0.010
	40%	0.208	0.137	0.198	0.208	0.176	0.011
	50%	0.230	0.160	0.223	0.231	0.198	0.012
PSNR	10%	32.810	44.450	34.712	32.745	38.856	56.263
	20%	31.643	39.202	33.204	31.885	35.670	55.500
	30%	30.668	36.171	31.639	30.587	33.269	54.872
	40%	29.403	33.941	29.981	29.365	31.352	54.204
	50%	28.143	32.131	29.008	27.915	29.704	53.305
SSIM	10%	0.897	0.975	0.926	0.893	0.927	0.100
	20%	0.808	0.921	0.837	0.805	0.834	0.100
	30%	0.700	0.861	0.732	0.701	0.725	0.999

	40%	0.601	0.808	0.631	0.604	0.631	0.999
	50%	0.516	0.757	0.550	0.522	0.558	0.999
Proposed metric	10%	43.023	45.468	43.710	43.580	43.787	64.913
	20%	41.921	44.447	42.435	42.510	42.490	64.360
	30%	41.507	43.726	41.791	41.626	41.795	64.061
	40%	40.927	43.022	41.084	41.000	41.134	63.824
	50%	40.308	42.372	40.870	40.211	40.438	63.470

4.8. Case study 8: Scenaric Image

In case study 8, the Scenaric image is taken as the input. After denoising, the obtained outputs are depicted in Figure 9. The noise-added image is shown in Figure 9(b), and the filtered output using the enhanced DWT is shown in Figure 9(c).

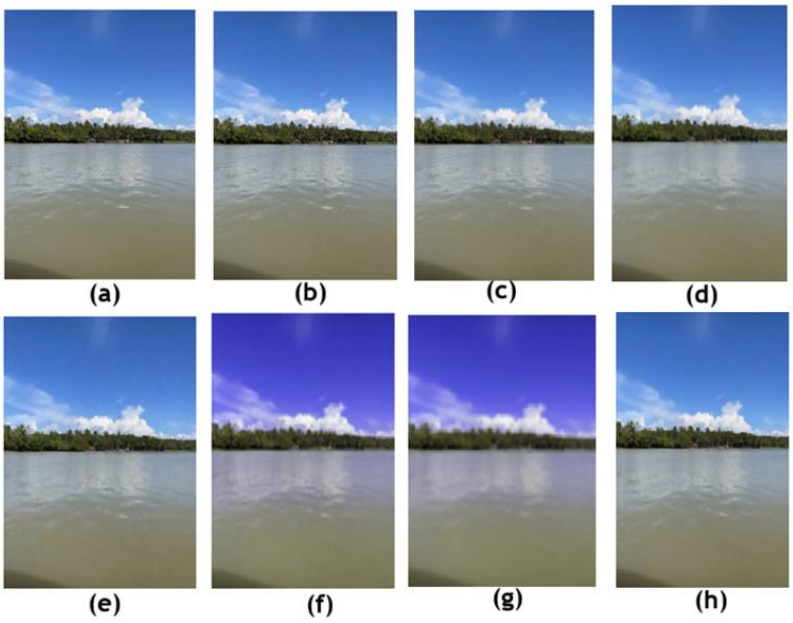

Figure 9: (a) Input image, (b) Noisy image, (c) Enhanced DWT, (d) BWT, (e) DWT, (f) Lee, (g) Frost, (h) Weiner

Likewise, the filtered outputs using existing transforms, such as the Berkeley Wavelet Transform (BWT), Standard DWT filter, Lee filter, Frost filter and Weiner filter, are shown in Figure 9(d-h), respectively. The performance of the various algorithms was analyzed using similarity metrics; the results are shown in Table 8.

Table 8: Existing and proposed metric values for the scenaric image

Parameter	Noise Level	DWT	BWT	Lee	Frost	Weiner	Proposed Method
NAE	10%	0.126	0.095	0.117	0.157	0.081	0.007
	20%	0.167	0.103	0.149	0.185	0.117	0.008
	30%	0.199	0.126	0.187	0.195	0.149	0.012
	40%	0.215	0.163	0.211	0.199	0.176	0.012
	50%	0.256	0.189	0.239	0.221	0.198	0.013
PSNR	10%	30.452	36.342	30.102	30.101	38.856	39.987
	20%	29.453	34.782	28.635	29.145	35.670	38.456
	30%	28.563	34.529	27.597	27.431	33.269	37.234
	40%	27.895	32.785	26.659	26.647	31.352	37.189
	50%	26.157	30.544	25.877	22.759	29.704	36.427
SSIM	10%	0.853	0.975	0.827	0.805	0.927	0.998
	20%	0.785	0.921	0.775	0.765	0.834	0.997
	30%	0.694	0.861	0.684	0.675	0.725	0.997
	40%	0.585	0.809	0.596	0.570	0.631	0.997

	50%	0.497	0.757	0.487	0.488	0.558	0.997
Proposed metric	10%	42.542	43.468	42.648	38.676	43.199	44.563
	20%	39.425	43.447	40.157	37.156	43.178	44.154
	30%	39.103	42.726	38.548	36.934	42.146	43.892
	40%	38.452	42.022	37.770	36.786	42.799	43.892
	50%	36.023	40.372	35.679	33.787	40.880	42.561

5. Conclusion

Denoising is a basic and essential step in image pre-processing and analysis, as it closely relates to the quality and reliability of subsequent computational activities. The correct extraction of information from images is crucial for accurate segmentation of specific image regions, effective identification of certain diseases, and accurate grading of the condition's severity. Noise in the image can significantly affect these processes, leading to misinterpretation or reduced diagnostic effectiveness. The proposed work provides a well-organized, comprehensive guideline for researchers to select a suitable filtering approach based on the properties of a particular image. This increases the overall accuracy and resilience of the subsequent stages in the image processing pipeline. Specifically, the proposed enhanced Discrete Wavelet Transform (DWT)- based denoising method exhibits excellent, consistent performance across a wide variety of images, including photos from publicly available datasets as well as photographs taken with ordinary camera devices. Moreover, the method is shown to be robust in both high- and low-noise environments, demonstrating its adaptability and generalizability. This adaptability allows one to employ the method with confidence in a variety of imaging settings. Finally, the proposed method outperforms the state-of-the-art denoising strategies.

Acknowledgment: The authors sincerely acknowledge the support and academic environment provided by Sri Krishna College of Engineering and Technology, Alliance University, S.A. Engineering College, SRM Institute of Science and Technology at Ramapuram, and Dhaanish Ahmed College of Engineering. Their contributions and institutional support were instrumental in the successful completion of this research.

Data Availability Statement: The data utilized in this study, related to the development of an intelligent noise suppression algorithm for multi-purpose imaging systems, are available from the corresponding authors upon reasonable request. Data sharing is subject to applicable ethical guidelines and institutional policies to ensure responsible use.

Funding Statement: The authors confirm that no financial support or external funding was received for the conduct, writing, or publication of this research work.

Conflicts of Interest Statement: All authors declare that there are no competing interests or conflicts that could have influenced the outcomes of this study. Proper acknowledgment of all referenced sources has been ensured.

Ethics and Consent Statement: Ethical approval for this study was obtained from the relevant institutional authority, and informed consent was secured from all participating organizations and individuals before data collection. The authors collectively affirm adherence to established ethical standards throughout the research process.

References

1. S. Gu, Q. Xie, D. Meng, W. Zuo, X. Feng, and L. Zhang, "Weighted nuclear norm minimization and its applications to low-level vision," *International Journal of Computer Mathematics*, vol. 121, no. 7, pp. 183–208, 2017.
2. P. Coupé, J. V. Manjón, E. Gedamu, D. Arnold, M. Robles, and D. L. Collins, "Robust Rician noise estimation for MR images," *Medical Image Analysis*, vol. 14, no. 4, pp. 483–493, 2010.
3. M. El Zein, W. El Laz, M. Laza, T. Wazzan, I. Kaakour, and Y. Abu Adla, "A deep learning framework for denoising MRI images using autoencoders," in *Proc. 2023 5th Int. Conf. on Bio-engineering for Smart Technologies (BioSMART)*, Paris, France, 2023.
4. S. Kollem, K. R. L. Reddy, and D. S. Rao, "Denoising and segmentation of MR images using fourth-order non-linear adaptive PDE and new convergent clustering," *International Journal of Imaging Systems and Technology*, vol. 29, no. 3, pp. 195–209, 2019.
5. J. V. Manjón, P. Coupé, and A. Buades, "MRI noise estimation and denoising using nonlocal PCA," *Medical Image Analysis*, vol. 22, no. 1, pp. 35–47, 2015.
6. E. G. Onyedinma and I. E. Onyenwe, "Image restoration: A comparative analysis in image de-noising using different spatial filtering techniques," *International Journal of Latest Technology in Engineering, Management and Applied Science*, vol. 12, no. 11, pp. 55–63, 2023.

7. A. Priya, K. Sinha, S. Choudhary, and S. Pridarshini, “Image denoising technique using various filter models: A survey,” in Proc. *2018 Int. Conf. on Computing, Power and Communication Technologies (GUCON)*, Greater Noida, India, 2018.
8. F. Ullah, K. Kumar, T. Rahim, J. Khan, and Y. Jung, “A new hybrid image denoising algorithm using adaptive and modified decision-based filters for enhanced image quality,” *Scientific Reports*, vol. 15, no. 3, pp. 1–29, 2025.
9. H. Xiao, B. Guo, H. Zhang, and C. Li, “A parallel algorithm of image mean filtering based on OpenCL,” *IEEE Access*, vol. 9, no. 3, pp. 65001–65016, 2021.
10. G. Capobianco, C. Cerrone, A. Di Placido, D. Durand, L. Pavone, D. D. Russo, and F. Sebastiano, “Image convolution: A linear programming approach for filter design,” *Soft Computing*, vol. 25, no. 4, pp. 8941–8956, 2021.
11. S. S. Mohanty and S. Tripathy, “Application of different filtering techniques in digital image processing,” *Journal of Physics: Conference Series*, vol. 2062, no. 11, pp. 1–7, 2021.
12. D. Jiang, W. Dou, L. Vosters, X. Xu, Y. Sun, and T. Tan, “Denoising of 3D magnetic resonance images with multi-channel residual learning of convolutional neural networks,” *Japanese Journal of Radiology*, vol. 36, no. 7, pp. 566–574, 2018.
13. T. Pieciak, S. Aja-Fernández, and G. Vegas-Sánchez-Ferrero, “Non-stationary Rician noise estimation in parallel MRI using a single image: A variance-stabilizing approach,” *IEEE Transactions on Pattern Analysis and Machine Intelligence*, vol. 39, no. 10, pp. 2015–2029, 2016.
14. T. Pieciak, F. Bogusz, A. Tristán-Vega, R. de Luis-García, and S. Aja-Fernández, “Single-shell return-to-the-origin probability diffusion MRI measure under a non-stationary Rician distributed noise,” in Proc. *2019 IEEE 16th Int. Symp. on Biomedical Imaging (ISBI)*, Venice, Italy, 2019.
15. S. Li, J. Zhou, D. Liang, and Q. Liu, “MRI denoising using progressively distribution-based neural network,” *Magnetic Resonance Imaging*, vol. 71, no. 9, pp. 55–68, 2020.
16. S. A. Akar, “Determination of optimal parameters for bilateral filter in brain MR image denoising,” *Applied Soft Computing*, vol. 43, no. 6, pp. 87–96, 2016.
17. R. Biswas, D. Purkayastha, and S. Roy, “Denoising of MRI images using curvelet transform,” in Advances in Systems, Control and Automation, *Springer*, Singapore, 2017.
18. P. Elahi, S. Beheshti, and M. Hashemi, “BM3D MRI denoising equipped with noise invalidation technique,” in *Proc. 2014 IEEE Int. Conf. on Acoustics, Speech and Signal Processing (ICASSP)*, Florence, Italy, 2014.
19. A. Garg and V. Khandelwal, “Despeckling of medical ultrasound images using fast bilateral filter and NeighShrinkSure filter in wavelet domain,” in Advances in Signal Processing and Communication. *Springer*, Singapore, 2019.
20. R. W. Liu, L. Shi, S. C. H. Yu, and D. Wang, “A two-step optimization approach for nonlocal total variation-based Rician noise reduction in MR images,” *Medical Physics*, vol. 42, no. 9, pp. 5167–5187, 2015.
21. M. Gandhi, C. Satheesh, E. S. Soji, M. Saranya, S. S. Rajest, and S. K. Kothuru, “Image recognition and extraction on computerized vision for sign language decoding,” in *Explainable AI Applications for Human Behavior Analysis, IGI Global*, United States of America, 2024.
22. L. Larxel, “Brain tumor segmentation,” Kaggle, 2021. [Accessed by 12/02/2025].